Endothelial Cells Proactively Form Microvilli-Like Membrane Projections upon Intercellular Adhesion Molecule 1 Engagement of Leukocyte LFA-1[1]

Christopher V. Carman, Chang-Duk Jun,[2] Azucena Salas, and Timothy A. Springer[3]

Specific leukocyte/endothelial interactions are critical for immunity and inflammation, yet the molecular details of this interaction interface remain poorly understood. Thus, we investigated, with confocal microscopy, the distribution dynamics of the central adhesion molecules ICAM-1 and LFA-1 in this context. Monolayers of activated HUVECs stained with fluorescent anti-ICAM-1 Fabs or Chinese hamster ovary-K1 cells expressing ICAM-1-green fluorescent protein were allowed to bind LFA-1-bearing monocytes, neutrophils, or K562 LFA-1 transfectants. ICAM-1 was rapidly relocalized to newly formed microvilli-like membrane projections in response to binding LFA-1 on leukocytes. These ICAM-1-enriched projections encircled the leukocytes extending up their sides and clustered LFA-1 underneath into linear tracks. Projections formed independently of VCAM-1/very late Ag 4 interactions, shear, and proactive contributions from the LFA-1-bearing cells. In the ICAM-1-bearing endothelial cells, projections were enriched in actin but not microtubules, required intracellular calcium, and intact microfilament and microtubule cytoskeletons and were independent of Rho/Rho kinase signaling. Disruption of these projections with cytochalasin D, colchicine, or BAPTA-AM had no affect on firm adhesion. These data show that in response to LFA-1 engagement the endothelium proactively forms an ICAM-1-enriched cup-like structure that surrounds adherent leukocytes but is not important for firm adhesion. This finding leaves open a possible role in leukocyte transendothelial migration, which would be consistent with the geometry and kinetics of formation of the cup-like structure. *The Journal of Immunology,* **2003, 171: 6135–6144.**

Leukocyte accumulation in inflammation and homing is a multistep process that involves rolling and firm adhesion on vascular endothelium and is culminated by transendothelial migration (TEM)[4] (1, 2). Initial rolling is mediated by selectin/glycosylated ligand interactions and has been mechanistically characterized in great detail. The subsequent arrest and adhesion strengthening of leukocytes on the endothelium is mediated by both ICAM-1/LFA-1 ($\alpha_L\beta_2$) and VCAM-1/very late Ag-4 (VLA-4; $\alpha_4\beta_1$) interactions, whereas TEM is mediated predominantly by ICAM-1 and LFA-1 (1, 3–8). Mechanisms for firm adhesion and TEM are not well defined. To improve our understanding of these events, details of the leukocyte/endothelial interaction interface and of the distribution dynamics of the key adhesion molecules, most notably ICAM-1 and LFA-1, must be elucidated.

In general, the cell surface distribution of integrins, such as LFA-1, appears to be modulated by interactions of their cytoplasmic domains with the actin cytoskeleton via direct binding to α-actinin, talin, vinculin, and paxillin (9). Importantly, engagement of ligand by integrins results in changes in these cytoskeletal interactions, promotion of integrin clustering, and activation of Rho family members, thereby regulating cell polarization and migration (9–11). It is not yet clear how these events are integrated in the context of leukocyte/endothelial interactions to produce firm adhesion and directional migration of leukocytes across the endothelium.

ICAM-1 is a member of the Ig superfamily of adhesion molecules, which is up-regulated on endothelial cells in response to inflammatory cytokines such as TNF-α (12). The short cytoplasmic domain of ICAM-1 interacts with the actin cytoskeleton via α-actinin, ezrin, and moesin, localizing it to cell surface microvilli (13–15). Ab-induced cross-linking and leukocyte-mediated clustering of ICAM-1 on endothelial cells initiates intracellular calcium flux and cytoskeletal signaling events including activation of the Rho GTPase and phosphorylation of cortactin, paxillin, p130cas, and focal-adhesion kinase (15–19). Treatment of the endothelium with either chelators of intracellular calcium, cytochalasin D, inhibitors of Rho signaling (16–18, 20–22), or colchicine (J. Greenwood and P. Adamson, personal communication) selectively inhibits leukocyte TEM, but not firm adhesion. Taken together, these and other studies have established a proactive role for ICAM-1 signaling/cytoskeletal interactions in facilitating TEM. While opening of interendothelial cell junctions has been suggested as one possible mechanism for the effects of ICAM-1 signaling on TEM (16–18, 20–22), the contribution of this and other potential mechanisms have yet to be clearly delineated.

The distribution of LFA-1 and ICAM-1 in the context of leukocyte/endothelial interactions has been partially characterized in several previous studies. One study, focused on LFA-1 and α-catenin, demonstrated a specific enrichment of LFA-1 in THP-1 cells

Department of Pathology, CBR Institute for Biomedical Research, Inc., Harvard Medical School, Boston, MA 02115

Received for publication May 16, 2003. Accepted for publication September 23, 2003.

The costs of publication of this article were defrayed in part by the payment of page charges. This article must therefore be hereby marked *advertisement* in accordance with 18 U.S.C. Section 1734 solely to indicate this fact.

[1] This work was supported by fellowships from the American Heart Association (to C.V.C.) and the Ministerio de Educación, Cultura y Deporte (to A.S.) and by Grant CA31798 the National Institutes of Health (to T.A.S.).

[2] Current address: Won Kwang University, South Korea.

[3] Address correspondence and reprint requests to Dr. Timothy A. Springer, CBR Institute for Biomedical Research, 200 Longwood Avenue, Boston, MA 02115. E-mail address: springeroffice@cbr.med.harvard.edu.

[4] Abbreviations used in this paper: TEM, transendothelial migration; BCECF, 2′,7′-bis-(2-carboxyethyl)-5-(and-6)-carboxyfluorescein; BDM, 2,3-butanedione monoxime; DIC, differential interference contrast; GFP, green fluorescent protein; I, inserted; MCP-1, monocyte chemoattractant peptide 1; PAF, platelet-activating factor; ROCK, Rho kinase; VLA-4, very late antigen 4; CHO, Chinese hamster ovary; TRITC, tetramethylrhodamine isothiocyanate.

0022-1767/03/$02.00

at the margin of the endothelial intercellular passage during TEM (23). In another study, HUVEC ICAM-1 was observed clustering into ring-shaped patterns underneath adherent monocytes (24). Recently, the distribution of HUVEC VCAM-1 and, to a lesser extent, ICAM-1 was examined during lymphocyte adhesion (25). This study demonstrated that VCAM-1/VLA-4 interactions promoted formation of endothelial projections that surrounded adherent lymphocytes and were enriched in VCAM-1, ezrin, and ICAM-1 (25). This later study provides particularly intriguing results, but also raises many new questions. Importantly, it remains to be established whether ICAM-1 redistribution occurs as a consequence of VCAM-1/VLA-4-driven events or whether ICAM-1/LFA-1 interactions actively participate in projection formation. In addition, the relative roles played by the leukocytes vs the endothelium in projection formation and the critical regulatory mechanisms for this are unknown. As well, the distribution of the leukocyte integrins in the context of endothelial projections has not been investigated. Finally, the functional role of this novel structure remains to be established. Although a potential role in adhesion strengthening was suggested (25), unambiguous experimental support for this hypothesis has not yet been presented.

Thus, in this study we used monolayers of Fab-stained, TNF-α-activated HUVECs and Chinese hamster ovary (CHO)-K1 cells expressing ICAM-1-green fluorescent protein (GFP) to characterize ICAM-1 distribution relative to that of LFA-1 during adhesion of a variety of leukocytes in the presence of both shear and chemoattractant. These studies reveal that the endothelium proactively generates microfilament-, microtubule-, and calcium-dependent ICAM-1-enriched cup-like structures within minutes of binding to LFA-1-bearing leukocytes. These structures appear not to function in adhesion strengthening, but could play a role in TEM.

Materials and Methods

Abs and reagents

Sources for the anti-human α_L and β_2 mAbs CBR-TS1/22, LFA1/2, CBR-LFA1/7, TS1/18, and YFC51.1 and anti-human ICAM-1 mAbs CBR-IC1/11, RR1 and R6.5; and anti-human VLA-4 mAb HP2/1 have been previously described (7, 13, 26, 27). Anti-human VCAM-1 mAbs BBIG-V1 and 1.G11B1 were obtained from R&D Systems (Minneapolis, MN) and RDI (Flanders, NJ), respectively. Anti-CD14-FITC and IgG2a-FITC Abs were purchased from Immunotech (Westbrook, ME). Fabs were prepared via papian cleavage using the ImmunoPure Fab Preparation kit (Pierce, Rockford, IL) according to the manufacturer's instructions. Ab and Fab conjugation to Cy3 (Amersham Pharmacia Biotech, Piscataway, NJ) or Alexa488 (Molecular Probes, Eugene, OR) bisfunctional dyes were according to the manufacturer's instructions, respectively. Monocyte chemoattractant peptide 1 (MCP-1) was obtained from BD PharMingen (San Diego, CA). Platelet-activating factor (PAF) and Y27632 were purchased from Calbiochem (La Jolla, CA). BAPTA-AM, 2,3-butanedione monoxime (BDM), colchicine, cytochalasin D, heparin, and tetramethylrhodamine isothiocyanate (TRITC)-phalloidin were obtained from Sigma-Aldrich (St. Louis, MO). Purified recombinant *Clostridium botulinum* C3 transferase was a gift kindly provided by Drs. J. Greenwood and P. Adamson (16).

Cells and cell culture

CHO-K1 cells were grown in RPMI 1640 (Life Technologies, Grand Island, NY) supplemented with 10% FBS, nonessential amino acids, and 50 μg/ml gentamicin. HUVECs were purchased from American Type Culture Collection (Manassas, VA) and maintained in medium 199 modified Earle's salt solution (Life Technologies) containing 20% FBS, 100 μg/ml endothelial growth supplement (Sigma-Aldrich), 1% Nutridoma NS (Roche; Indianapolis, IN), and 100 μg/ml heparin. HUVECs were grown on either plastic or glass surfaces precoated with 10 μg/ml fibronectin (Life Technologies) and used for no more than five passages. Cells were cultured at 37°C in humidified air containing 5% CO_2. Generation and maintenance of K562-LFA-1, K562-LFA-1-open, K562-LFA-1-closed, and K562-LFA-1-I-open were previously described (27, 28). Neutrophils and PBMC were prepared by standard Ficoll-Hypaque (Sigma-Aldrich) buoyant density centrifugation (29). Monocytes were prepared from PBMC by discontinuous Percoll (Amersham Pharmacia Biotech) gradient centrifugation (29). The purity of the resultant monocytes was routinely ~70%, as determined by anti-CD14-FITC and IgG2a-FITC (10 μg/ml) mAb staining followed by flow cytometry.

cDNA constructs and cell transfections

To generate ICAM-1 fused to GFP at its C terminus, the stop codon of ICAM-1 was replaced with a *Sac*II restriction site through PCR of the entire coding region of ICAM-1. The resultant PCR product was digested with *Hind*III and *Sac*II and subcloned into the pEGFP-N1 vector (Clontech Laboratories, Palo Alto, CA), thus giving rise to the plasmid IC1-GFP. The amino acid sequence of the linker spanning from the C terminus of ICAM-1 to the N terminus of enhanced GFP was PRARNPPVAT. Stable CHO-K1 transfectants expressing ICAM-1-GFP were established by FuGENE 6 (Roche) transfection of IC1-GFP DNA according to the manufacturer's instructions, followed by selection with 1 mg/ml geneticin (Life Technologies) beginning at 48 h posttransfection. The resultant stable cell line (CHO-IC1-GFP) was maintained in complete medium supplemented with the same concentrations of antibiotic. For transient cotransfections, 35-mm dishes of CHO-K1 cells were combined with 2 μg of pAPRM8-ICAM-1 and 2 μg of either pEGFP-actin or pEGFP-tubulin (Clontech Laboratories) and 60 μl of FuGENE 6 transfection reagent according to the manufacturer's instructions. Experiments were conducted 48 h posttransfection.

Preparation of Ab-coated beads

Polystyrene beads (14 μm in diameter; Bangs Laboratories, Carmel, IN) were washed once with PBS and then combined with 100 μg/ml purified R6.5 or YCF5.1 mAb at room temperature with rocking for 6 h. BSA at a final concentration of 1 mg/ml was then added and the mixture was incubated for an additional 2 h followed by washing six times in PBS. Beads were either used immediately or stored at 4°C for several days before use.

Adhesion imaging experiments

For most fluorescence microscopy experiments CHO-K1, CHO-IC1-GFP, or HUVEC cells were grown on polystyrene 35-mm cell culture dishes or on glass surfaces of either the ΔT4 or FCS2 live cell imaging chambers (Bioptechs, Butler, PA). CHO-K1 cells were plated at 50% confluency and used within 24 h. HUVECs were plated at 90% confluency and cultured for 48–72 h before use. Before each experiment, HUVECs were activated for 15 h with TNF-α (100 ng/ml; Invitrogen, Carlsbad, CA), which typically induced a 25- to 30-fold increase in ICAM-1 expression, as determined by staining with CBR-IC1/11-Fab conjugated to Alexa488 (CBR-IC1/11-Fab-488). Immediately before addition of leukocytes, HUVECs were incubated with CBR-IC1/11-Fab-488 or -Cy3 (20 μg/ml) and, based on previously described methods (30), either PAF (100 nM) or MCP-1 (200 ng/ml) at 37°C for 20 min. Where indicated, HUVECs or CHO-IC1-GFP cells were also preincubated with BAPTA-AM (20 μM, 1 h), colchicine (10 μM, 20 min), cytochalasin D (200 nM, 20 min), C3 transferase (50 μg/ml, 16 h), Y27632 (30 or 90 μM, 1 h), or the equivalent amount of vehicle (DMSO, 1 h) concomitant with Fab and chemoattractant. In all cases, CHO-IC1-GFP and HUVECs were washed five times before addition of leukocytes with HBSS supplemented with 20 mM HEPES (pH 7.2) and 1% human serum albumin (buffer A) and then cultured in buffer A with either 1 mM Ca^{2+}/Mg^{2+} or 1 mM Mn^{2+}. Although MCP-1 modestly improved monocyte/endothelial interactions, the presence of PAF enhanced neutrophil/HUVEC interactions 2- to 3-fold. The modest effects of MCP-1 compared with those of PAF may represent differences in the efficiency of "capture" of PAF, a lipid, vs MCP-1, a peptide, on the monolayer or the fact that TNF-α-activated endothelial cells are known to synthesize and secrete MCP-1 themselves, such that exogenous MCP-1 may be superfluous. LFA-1-bearing leukocytes or mAb-coated beads were washed and resuspended in buffer A with either 1 mM Ca^{2+}/Mg^{2+} or 1 mM Mn^{2+}before addition to monolayers. Where indicated, leukocytes were pretreated with either BDM (5 mM), cytochalasin D (2 μM), or vehicle (DMSO) for 30 min and then washed five times. Leukocytes or mAb-coated latex beads were then added to either CHO-IC1, CHO-IC1-GFP, or HUVEC monolayers and incubated at 37°C. For blocking experiments, either TS1/18, RR1/1, HP2/1, BBIG-V1, or 1.G11B1 mAbs (each at 20 μg/ml) or EDTA (5 mM) were preincubated with cells for 10 min before addition of leukocytes and were present during the coincubation. Cells were either imaged live in ΔT4 or FCS2 cell culture chambers maintained at 37°C or fixed (3.7% formaldehyde in PBS for 5 min), stained for LFA-1 (CBR-LFA1/7-Cy3; 20 μg/ml) or F-actin (TRITC-phalloidin; 2 μg/ml) in PBS for 20 min at room temperature, and then washed three times with PBS.

For shear experiments, CHO-IC1-GFP or HUVEC monolayers were assembled as the lower wall in a parallel-wall flow chamber, which was mounted on a thermoplate (Tokai Hit, Shizuaka-ken, Japan) to maintain

cells at 37°C. Chambers were perfused briefly with buffer A at 37°C using a syringe pump (Harvard Apparatus, Holliston, MA). Subsequently, leukocytes in buffer A with either 1 mM Ca^{2+}/Mg^{2+} or 1 mM Mn^{2+} were infused for 30 s at a wall shear stress of 0.3 dyne/cm^2 to allow accumulation. Then buffer A with the same cations was infused at 4 dyne/cm^2 for 20 min. Finally, cells were fixed by perfusion with PBS/3.7% formaldehyde for 5 min and washed by perfusion with PBS for 5 min, both at 4 dyne/cm^2. Cells were then stained as described above.

Quantitative adhesion assays

To quantitate adhesion, TNF-α-activated HUVECs and CHO-IC1-GFP monolayers grown in 96-well cell culture dishes were pretreated with blocking Abs, cytochalasin D, colchicine, or BAPTA-AM, as above, and then incubated with 5×10^4 2′,7′-bis-(2-carboxyethyl)-5-(and-6)-carboxyfluorescein (BCECF) acetoxymethyl ester (Molecular Probes)-labeled monocytes or K562-LFA-1 cells for 20 min at 37°C in buffer A with 1 mM Ca^{2+}/Mg^{2+}. Plates were read on a fluorescence concentration analyzer (Pandex Labs, Mundelein, IL) both before and after eight 200-μl washes with buffer A. Wells in which no leukocytes were added were used to measure background fluorescence of the monolayer. Adhesion was calculated as the background subtracted post-wash divided by the background-subtracted prewash signals (averaged from triplicate wells) multiplied by 100%.

For controlled detachment, CHO-IC1-GFP monolayers were prepared in a Bioptechs flow chamber, as described above, and BCECF-labeled K526-LFA1 cells at 2×10^6/ml were infused for 1 min at 0.3 dyne/cm^2. Shear was then stopped and cells were allowed to adhere for 20 min at 37°C. Fluorescence images of eight randomly selected fields were acquired during the adhesion and the number of cells per field was counted and averaged (input). Since BCECF signal intensity was >100 times that of ICAM-1-GFP, adherent K562-LFA-1 cells were unambiguously differentiated from the monolayer. Cells were then subjected to a shear regiment of 4 min each of 16, 32, and 64 dyne/cm^2 shear to detach the adherent cells. The average number of cells remaining per field was then quantified, divided by the input value, and multiplied by 100% to obtain the percent adhesion.

Imaging acquisition and processing

Wide-field differential interference contrast (DIC) and fluorescence imaging was conducted on a Zeiss Axiovert S100 epifluorescence microscope (Zeiss, Oberkochen, Germany) using either a ×40 or ×63 oil objective, coupled to a Hamamatsu Orca charge-coupled device (Middlesex, NJ). Confocal imaging was performed with a Bio-Rad Radiance 2000 laser-scanning confocal system (Bio-Rad, Hercules, CA) on an Olympus BX50BWI microscope (Melville, NY) with a ×100 water immersion objective. For serial Z-stacks, the section thickness ranged from 0.1 to 0.3 μm. Image processing, including background subtraction and digital deconvolution, was performed with Openlab software (Improvision, Lexington, MA). Three-dimensional reconstruction and projection of Z-stacks was performed with VoxBlast software (Vay Tek, Fairfield, IA). Images were then exported to Photoshop software (San Jose, CA) for preparation of final images.

Results

ICAM-1-bearing cells rapidly form ring-like clusters of ICAM-1 on binding leukocytes bearing activated LFA-1

To visualize the distribution of ICAM-1 during leukocyte adhesion, we generated CHO-K1 cells that stably express ICAM-1 fused to GFP through a 10-residue linker (CHO-IC1-GFP). In the absence of leukocytes, the ICAM-1-GFP was distributed across the apical surface of the CHO-K1 cells primarily into microvilli, which appear as puncta at low resolution. To CHO-IC1-GFP cell monolayers were added K562 cells that stably express either wild-type LFA-1 (K562-LFA-1) or LFA-1 containing the inserted (I) domain locked in the closed conformation with an introduced disulfide bond (K562-LFA-1-closed) (27). Cells were incubated in the presence of 1 mM Mn^{2+}, which activates wild-type but not locked closed LFA-1, at 37°C for 20 min and then imaged by live cell fluorescence microscopy. The K562-LFA-1-closed cells failed to perturb the ICAM-1 distribution (Fig. 1*A*). Similar results were obtained with K562-LFA-1 cells in the presence of nonactivating 1 mM Ca^{2+}/Mg^{2+} cations (data not shown). In contrast, Mn^{2+}-activated K562-LFA-1 cells induced a dramatic clustering of the ICAM-1-GFP into ring-shaped patterns (Fig. 1*B*) reminiscent of

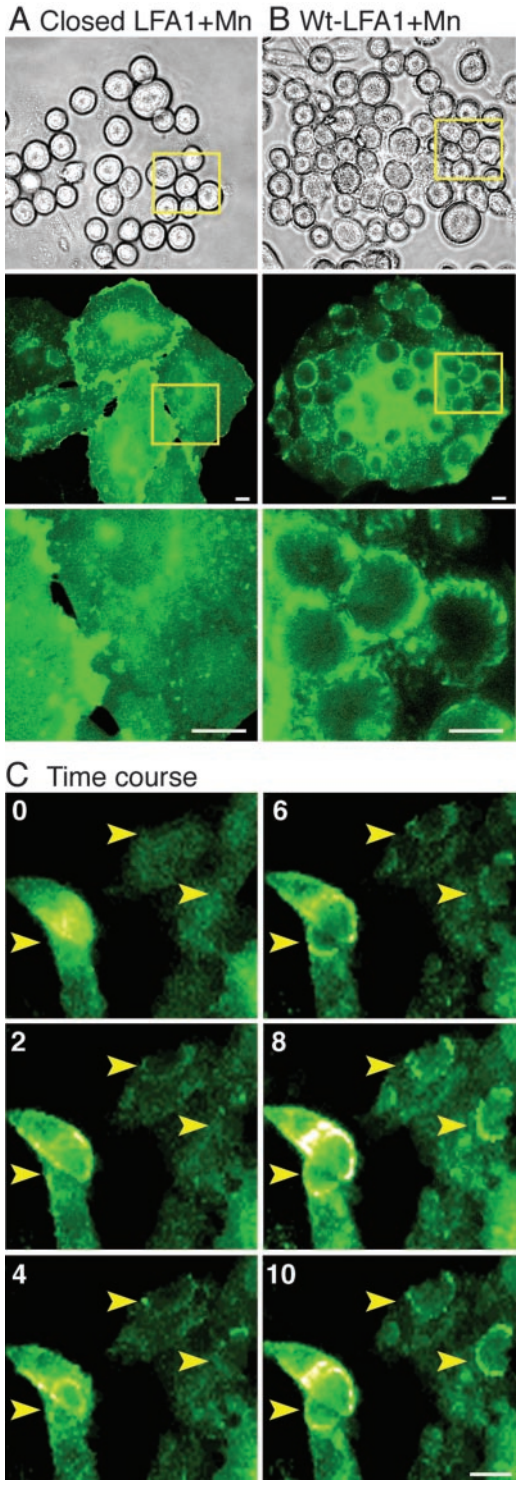

FIGURE 1. ICAM-1 rapidly forms ring-shaped clusters upon binding leukocytes bearing activated LFA-1. *A* and I,. CHO-IC1-GFP monolayers were incubated with K562-LFA-1-closed (*A*) or K562-LFA-1 (*B*) cells in the presence of 1 mM Mn^{2+} for 20 min at 37°C and then imaged live. Representative DIC (*upper panels*) and fluorescence microscopy (*middle* and *lower panels*) images are shown. *Lower panels*, A magnification of the boxed regions shown in the *middle panels*. *C*, CHO-IC1-GFP monolayers were incubated with K562-LFA-1-open cells with 1 mM Ca^{2+}/Mg^{2+} and live cell time-lapse imaging was performed at 37°C. Selected images at 0, 2, 4, 6, 8, and 10 min of coculture from a representative experiment are shown. Arrowheads indicate location of three separate K562 cells adherent to the monolayer. Scale bars, 10 μm.

ICAM-1-clustering patterns previously observed during HUVEC/monocyte interactions (24). Similar results were produced in 1 mM Ca^{2+}/Mg^{2+} by K562-LFA-1 cells activated with the Ab CBR-LFA1/2 (data not shown) and by K562 cells stably expressing constitutively active, locked open LFA-1 (K562-LFA-1-open) (27) (Fig. 1*C*). This redistribution was inhibited by function blocking Abs RR1/1 to ICAM-1 and TS1/18 to the integrin β_2 subunit (see Fig. 7 below) and by EDTA (data not shown). K562-LFA-1-dependent redistribution patterns of wild-type ICAM-1 in CHO-K1 cells, visualized by staining with an anti-ICAM-1 Fab directly conjugated to Alexa488 (CBR-IC1/11-Fab-488), were identical to those of ICAM-1-GFP (data not shown), demonstrating that ICAM-1 distribution was unaffected by the GFP tag. These data demonstrate that specific engagement by activated cell surface LFA-1 is sufficient to drive redistribution of ICAM-1 into ring-shaped clusters.

To assess the kinetics of this redistribution, live cell time-lapse imaging was performed with the CHO-IC1-GFP/K562-LFA-1-open system (Fig. 1*C*). ICAM-1-GFP redistribution was typically apparent within 1–2 min after addition of K562-LFA-open cells and largely plateaued by ~10 min. (Fig. 1*C*). However, some enrichment of ICAM-1 clusters continued with slower kinetics over the next 50 min and then remained relatively stable over the next hour (Fig. 2 and data not shown).

ICAM-1 "clusters" represent ICAM-1-enriched microvilli-like vertical membrane projections

High-resolution confocal microscopy coupled to digital deconvolution and three-dimensional image reconstruction revealed that the ring-shaped ICAM-1 clusters were actually well-defined ICAM-1-enriched microvilli-like vertical membrane projections that formed cup-like structures that encircled the K562-LFA-1 cells, extended up their sides, and often approached their apex (Fig. 2). The average length of the projections was ~5 μm at 5 min (Fig. 2*B*), ~10 μm at 20 min (Fig. 2, *A* and *C*), and ~12 μm at 60 min (Fig. 2*D*). At early time points, projections had the appearance of elongated microvilli (Fig. 2*B*), while at later time points longer, and often broader, projections formed which exhibited varying degrees of branching (Fig. 2, *A*, *C*, and *D*).

To examine more physiologic ICAM-1-expressing cells, HUVECs were activated with TNF-α to induce expression of ICAM-1. The monolayers were stained with CBR-IC1/11-Fab-488 and visualized by live cell confocal microscopy. mAb CBR-IC1/11 is directed toward domains 3 and 4 of ICAM-1 and does not block binding to LFA-1, although it does interfere with binding of the integrin Mac-1 ($\alpha_M\beta_2$) (26). The basal distribution of ICAM-1 in HUVECs was similar to that seen with the CHO-IC1-GFP cells. Addition of K562-LFA-1 cells in Mn^{2+} (Fig. 3*A*) or K562-LFA-1-open cells in Ca^{2+}/Mg^{2+} (data not shown) led to formation of ICAM-1-enriched projections with similar architecture and kinetics as seen with CHO-IC1-GFP cells. Formation of projections was inhibited by mAbs RR1/1 to ICAM-1 and TS1/18 to the integrin β_2 subunit or by EDTA (data not shown).

To examine projection behavior in the presence of physiologic LFA-1-bearing cells, TNF-α-activated HUVECs were incubated with freshly isolated human monocytes and neutrophils. HUVEC monolayers were treated with MCP-1 before addition of monocytes or PAF before addition of neutrophils. Chemoattractant not associated with the monolayer was removed by washing before addition of leukocytes. Under these conditions, the majority of the adherent leukocytes were associated with ICAM-1-enriched projections. Often the projections surrounding the neutrophils and monocytes extended up the sides, curved over the tops of the leukocytes, and ended in a more horizontal orientation, reflecting the more spread shape of the neutrophils and monocytes (Fig. 3, *B* and *C*), contrasting the primarily vertical projections formed around the spherical K562-LFA-1 cells (Fig. 3*A*).

LFA-1 is clustered under ICAM-1-enriched projections

The distribution of LFA-1 in K562-LFA-1 cells and both LFA-1 and Mac-1 in neutrophils and monocytes adherent to HUVEC monolayers was examined by staining with the Cy3-conjugated Ab CBR-LFA1/7 (CBR-LFA1/7-Cy3), which is specific for the β_2 subunit. β_2 was partially clustered at the bottom of K562-LFA-1

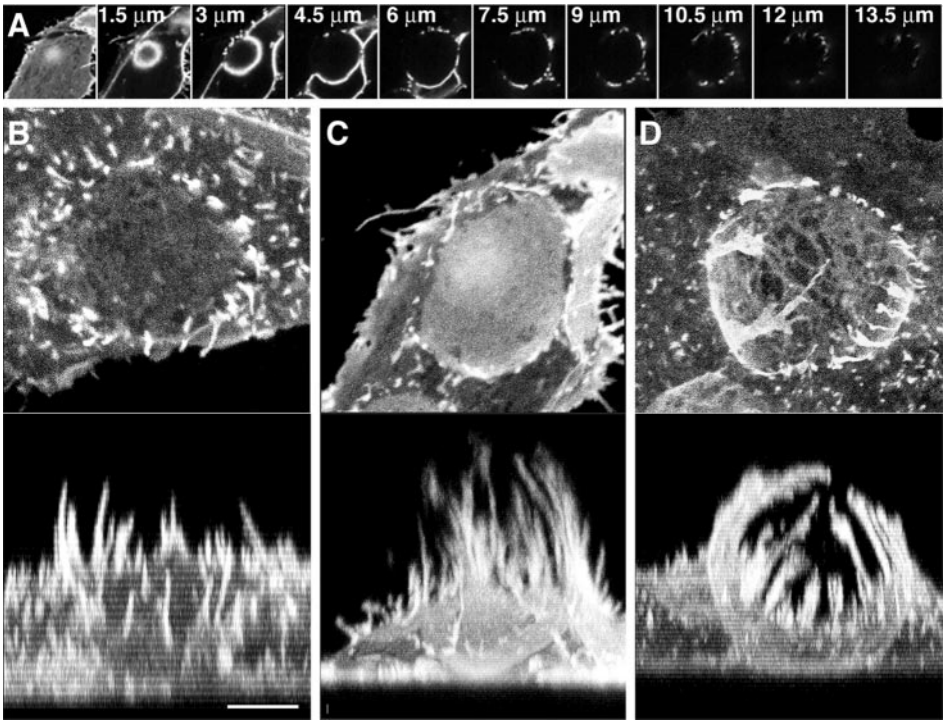

FIGURE 2. ICAM-1 clusters represent vertical ICAM-1-enriched microvilli-like membrane projections. CHO-IC1-GFP monolayers were incubated with Mn^{2+}-activated K562-LFA-1 cells for varied times and then imaged by live cell confocal microscopy. Serial Z-sections were acquired and subjected to digital deconvolution and three-dimensional image reconstruction. All images represent the ICAM-1-GFP distribution at the location of an adherent K562-LFA-1 cell, as confirmed by DIC imaging (data not shown). *A*, Selected Z-sections, depicting 1.5-μm intervals, from the most basal surface (*left*) to the most apical surface (*right*) of a representative 20-min incubation. The same cell is shown in *C*. *B–D*, Digital reconstructions of complete Z-series were rendered either en face (i.e., top view, *upper panel*) or after 90° rotation about the *x*-axis (i.e., side view, *lower panel*. *B–D*, Representative cells after 5-, 20-, and 60-min incubations, respectively. Scale bar, 5 μm.

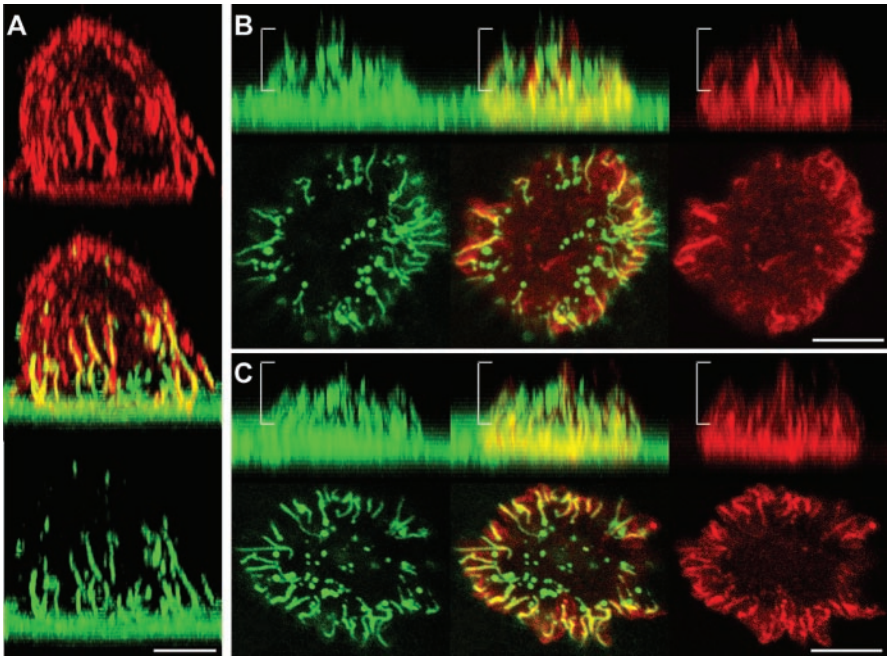

FIGURE 3. ICAM-1 projections induce linear clusters of LFA-1 along the sides of leukocytes. Mn^{2+}-activated K562-LFA-1 cells (*A*), neutrophils in the presence of PAF (*B*), or monocytes in the presence of MCP-1 (*C*) were incubated with TNF-α-activated, CBR-IC1/11-Fab-488-stained HUVECs (green) for 20 min at 37°C followed by fixation and staining with CBR-LFA1/7-Cy3 mAb to the β_2-integrin subunit (red). Regions of colocalization appear yellow. *A,* Side view of a three-dimensional projection of a representative K562-LFA-1-open cell/HUVEC adhesion. *B* and *C,* Side views (*upper*) and top views (*lower*) of neutrophil/HUVEC (*B*) and monocyte/HUVEC (*C*) adhesions. To more clearly view the structures in the upper portions of the adherent leukocytes, the top views were generated by projecting only the Z-sections that represent the most apical half of the specimens (brackets). Scale bars, 5 μm.

cells, neutrophils, and monocytes, where they contacted the apical surface of the HUVECs. Furthermore, robust patterns of β_2 clusters were observed along the sides of the leukocytes colocalized with the endothelial ICAM-1 projections (Fig. 3). The vertical tracks of the ICAM-1 projections along the sides of the K562-LFA-1 cells were mirrored by linear clusters of β_2 (Fig. 3*A*). For the more spread neutrophils and monocytes, linear clusters of β_2 were apparent in both top and side views and curved over the tops of these cells alongside the ICAM-1 projections (Fig. 3, *B* and *C*). It is interesting that β_2 and ICAM-1 were codistributed along the lengths of the projections, whereas at the tips of the projections over the center of the cells, ICAM-1 but not β_2 was present.

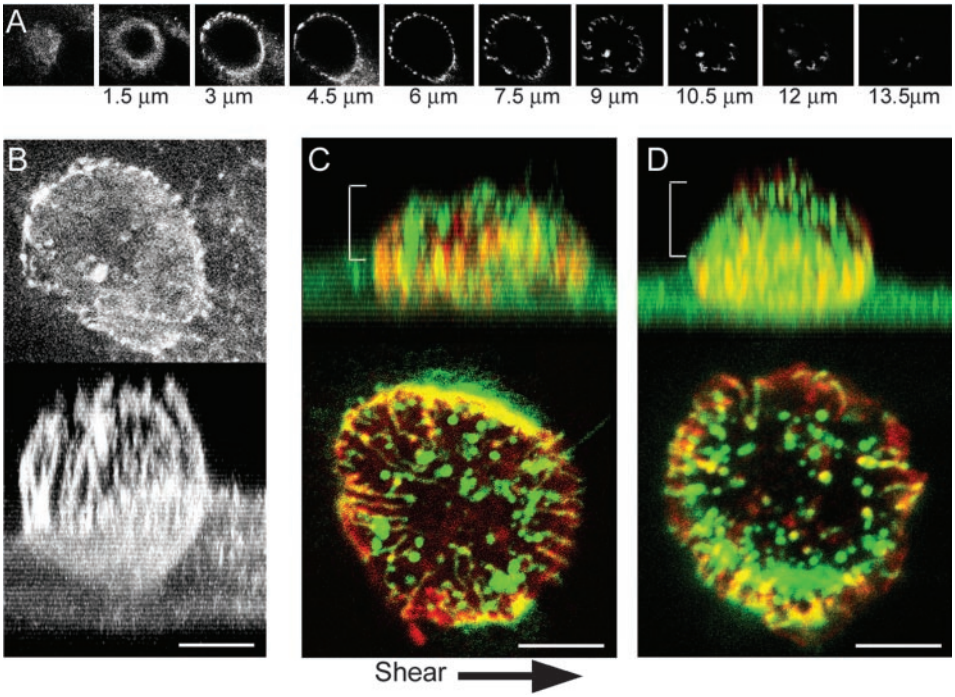

FIGURE 4. ICAM-1 projections form independently of shear stress. CHO-IC1-GFP and Mn^{2+}-activated K562-LFA-1 cells (*A* and *B*) or PAF (*C*)- or MCP-1 (*D*)-pretreated, TNF-α-activated HUVECs and either neutrophils (*C*) or monocytes (*D*) were incubated together for 20 min under a shear force of 4 dyne/cm^2 and then fixed and imaged as described in *Materials and Methods*. *A,* Selected Z-sections from a representative CHO-IC1-GFP/K562-LFA-1 adhesion depicting ICAM-1 GFP distribution at 1.5-μm intervals, from the most basal surface (*left*) to the most apical surface (*right*). *B,* A digital reconstruction of the complete Z-series of the specimen shown in *A* was rendered to generate top (*upper*) and side (*bottom*) views. Compare *A* and *B* with Fig. 2, *A* and *C*. *C* and *D,* Side (*upper*) and top (*lower*) views of HUVEC/neutrophil (*C*) or HUVEC/monocyte (*D*) adhesions, respectively. CBR-LFA1/7-Cy3 (red) and CBR-IC1/11-Fab-488 (green) staining reveal leukocyte LFA-1 and HUVEC ICAM-1, respectively. Top views were generated from only the apical half of the Z-series (brackets). Compare *C* and *D* with Fig. 3, *B* and *C*. Arrow indicates the direction of the shear force applied. Scale bars, 5 μm.

Whether these represent sites of internalization of β_2 in the leukocytes is not known.

Projections form independently of shear stress

To determine whether the formation of ICAM-1-enriched projections is altered by physiologic shear flow, we characterized leukocyte binding to monolayers of CHO-IC1-GFP- and TNF-α-activated HUVECs in a parallel wall flow chamber. Mn^{2+}-activated K562-LFA-1 cells were accumulated on monolayers of CHO-IC1-GFP mounted on the bottom wall of the flow chamber for 30 s at 0.3 dyne/cm^2 and then subjected to a constant shear force of 4 dyne/cm^2 for 20 min. Monocytes and neutrophils were similarly accumulated on either MCP-1- or PAF-treated HUVECs and then subjected to 4 dyne/cm^2 shear force for 20 min. Cells were then fixed under shear and imaged by confocal microscopy. In the presence of shear flow, the formation of projections and the distribution of ICAM-1 and LFA-1 (Fig. 4) was indistinguishable from that in the absence of shear (Figs. 2 and 3).

Projections are independent of any proactive contribution from the LFA-1-bearing cells

To determine whether the leukocytes play an obligate proactive role in the formation of ICAM-1-enriched endothelial projections, we examined the effects of perturbation of the LFA-1 cytoplasmic domain/cytoskeletal interface in K562 cells. Thus, K562-LFA-1 cells were pretreated with BDM, a specific inhibitor of actin contractility, or cytochalasin D, a specific inhibitor of microfilament assembly, and then washed and incubated with CHO-IC1-GFP cells. Both of these treatments failed to produce any detectable differences in the ICAM-1-GFP redistribution patterns (Fig. 5, *B* and *C*) and projections (data not shown) compared with controls (Fig. 5*A*), suggesting that a functional LFA-1 cytoplasmic domain/cytoskeletal link may be dispensable for projection formation. To test this directly, we examined K562 cells with cell surface expression of the locked open, LFA-1 ligand-binding I domain, isolated from other domains in $\alpha_L\beta_2$, and expressed on the cell surface attached to the transmembrane domain and first five residues of the cytoplasmic domain of the platelet-derived growth factor receptor, which is not thought to interact with the cytoskeleton (K562-LFA-1-I-open) (28). These cells promoted ICAM-1 redistribution patterns (Fig. 5*D*) and projections (data not shown) in CHO-IC1-GFP cells that were indistinguishable from those formed around K562 cells bearing full-length LFA-1 (Fig. 5A). Finally, we examined whether cells were required at all for the formation of projections by substituting the K562-LFA-1 cells with similar-sized latex beads coated with Abs. Addition of beads coated with ICAM-1 mAb R6.5 (Fig. 5*E*), but not control mAb YFC51.1 (Fig. 5*F*), readily elicited projections in activated HUVECs. These projections took on a somewhat more lamellar morphology (Fig. 5*E*), possibly as a consequence of differences in the distribution/density of the Ab compared with that of cell surface LFA-1.

ICAM-1 projections are enriched in actin

To characterize the cytoskeletal elements present in the projections, CHO-K1 cells were cotransfected with wild-type ICAM-1 and either GFP-actin or GFP-tubulin. This approach, unlike staining methods, allowed us to selectively visualize the microfilament and microtubule systems of the CHO-K1 cells during adhesion of leukocytes. In live cell experiments, GFP-actin was clearly observed to be enriched in the ICAM-1 projections (Fig. 6, *A* and *B*). Some degree of microtubule rearrangement was observed in the CHO-K1 cells in proximity of the bound K562-LFA-1 cells (Fig. 6*C*); however, a specific enrichment of GFP-tubulin in the projections was not detected (data not shown).

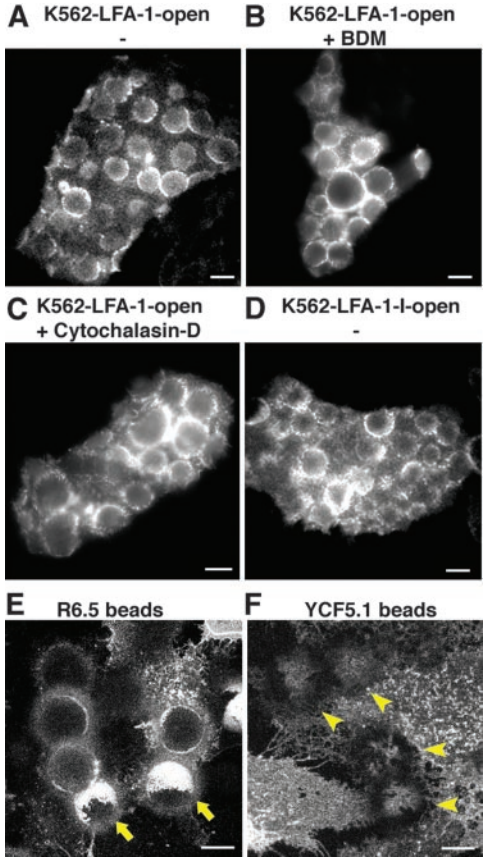

FIGURE 5. ICAM-1 projections form independently of any proactive contribution from leukocytes. *A–D,* CHO-IC1-GFP cells were incubated with K562-LFA-1-open cells (*A–C*) or K562-LFA-1-I-open cells (*D*) for 20 min at 37°C before visualization by live cell fluorescence microscopy. K562-LFA-1-open cells were pretreated with either DMSO (−) (*A*), 5 mM BDM (*B*), or 2 μM cytochalasin D (*C*) for 30 min at 37°C and then washed immediately before addition to CHO-IC1-GFP cells. Representative fluorescence images are shown. *E* and *F*, TNF-α-activated, CBR-IC1/11-Fab-488-stained HUVECs were incubated with 14-μm latex beads coated with R6.5 mAb to ICAM-1 (*E*) or YFC51.1 control mAb (*F*) at 37°C for 20 min and then viewed by live cell confocal microscopy. Representative top view projections are shown. Arrowheads in *F* indicate the location of four YFC51.1 beads settled on the HUVECs. Adjacent dark rings represent diffraction of the IC1/11-Fab-488 fluorescence in the region directly below the beads (*F*). Bright ring-like patterns of ICAM-1 apparent at the periphery of most R6.5 mAb beads (*E*) represent fluorescence in more apical sections that masks the more basal "dark rings" seen with YFC51.1 mAb beads. Arrows in *E* indicate projections associated with broad lamella that partially extended over the tops of two beads. Scale bars, 10 μm.

To further examine microfilaments, we bound R6.5-coated latex beads to HUVECs and fixed and stained them with TRITC-phalloidin. Since the beads are devoid of TRITC-phalloidin staining, unlike the LFA-1-bearing cells, we were able to visualize the HUVEC microfilaments unambiguously. ICAM-1 projections/lamella extended over the tops of the latex beads, and TRITC-phalloidin staining revealed clear bundles of microfilaments in these projections/lamella (Fig. 6*D*). These data demonstrate that the projections are selectively enriched in actin.

Projections are dependent on ICAM-1/LFA-1 binding, microfilaments, microtubules, and calcium signaling and are independent of Rho/ROCK activity.

To quantitatively establish the role of ICAM-1/LFA-1 interactions in projection formation, we carefully visualized >100 adherent

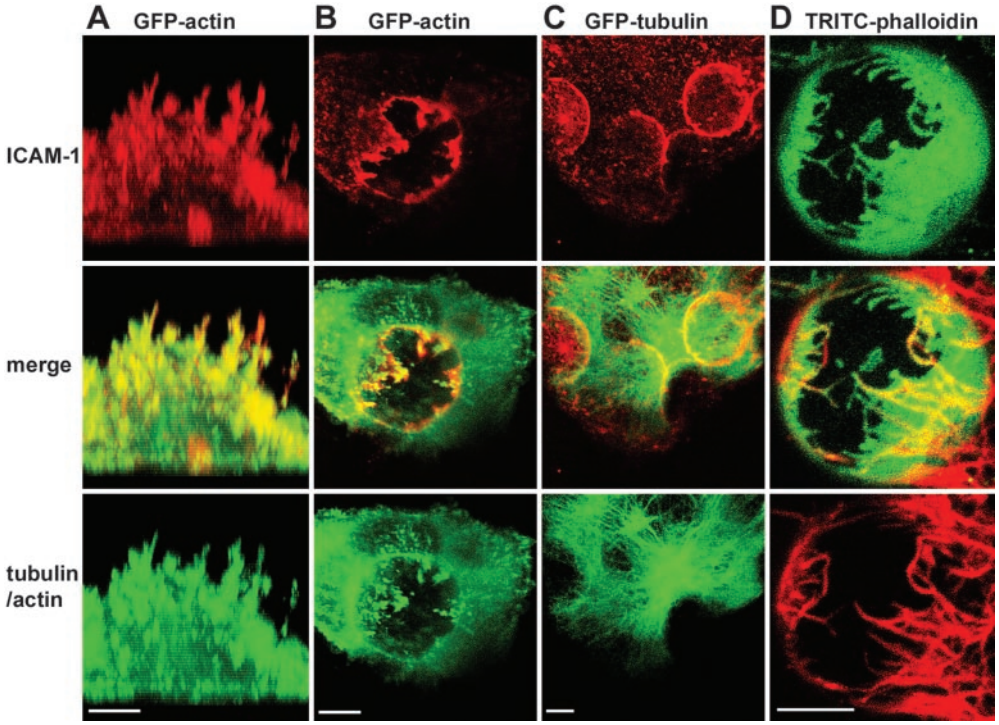

FIGURE 6. ICAM-1 projections are enriched in actin. *A–C*, CHO-K1 cells were transiently cotransfected with ICAM-1 and either GFP-actin (green, *A* and *B*) or GFP-tubulin (green, *C*). Transfectants were labeled with CBR-IC1/11-Fab-Cy3 (red), incubated with Mn^{2+}-activated K562-LFA-1 for 20 min at 37°C, and then imaged by live cell confocal microscopy. Representative images depicting either side (*A*) or top (*B* and *C*) views are shown. *D*, TNF-α-activated, CBR-IC1/11-Fab-488-stained HUVECs (green) were incubated with R6.5-coated latex beads for 20 min before fixation and stained with TRITC-phalloidin (red). A representative top view projection of the apical half of the specimen is depicted. Scale bars, 5 μm.

cells, from randomly selected fields and from separate experiments, in all Z-sections and scored them for the presence of associated ICAM-1-enriched projections. Nearly 70% of the CBR-LFA1/2-activated K562 cells bound to CHO-IC1-GFP cells (Fig. 7*A*), and ~75% of the MCP-1-activated monocytes bound to HUVECs (Fig. 7*B*) were associated with ICAM-1-enriched projections. In both cases, projections were almost completely blocked by the addition of function-blocking mAbs RR1/1 to ICAM-1 and TS1/18 to integrin β_2 (Fig. 7, *A* and *B*). Importantly, blockade of VLA-4 and VCAM-1 interactions with the function blocking Abs HP2/1, BBIG-V1, and 1.G11B1 had little effect on ICAM-1 projections formed in response to monocyte/HUVEC interactions (Fig. 7*B*), demonstrating that these adhesion receptors are not required for ICAM-1 projection formation.

Intracellular calcium flux, cytoskeletal rearrangement, and Rho signaling are central events initiated by ICAM-1 clustering (15–22, 24). To assess whether these events are required for projection formation, HUVECs and CHO-IC1-GFP cells were pretreated with BAPTA-AM to chelate intracellular calcium, cytochalasin D to disrupt actin microfilaments, colchicine to disrupt microtubules, C3 transferase to inhibit Rho function, or Y27632 to inhibit Rho kinase (ROCK) activity. Compared with vehicle controls, BAPTA-AM, cytochalasin D, and colchicine all dramatically attenuated ICAM-1 clustering and projection formation around K562-LFA-1 cells (Fig. 7, *A*, *C*, and *D*) and monocytes (Fig. 7, *B* and *E*), leading to much more planar adhesion interfaces. These results demonstrate that calcium signaling and intact microtubule and microfilament cytoskeletons are all required in the endothelium for efficient ICAM-1 projection formation. Furthermore, under these conditions the linear clusters of LFA-1 along the sides of the leukocytes were absent (Fig. 7*E*), demonstrating their dependence on the ICAM-1 projections. In contrast, C3 pretreatment of HUVECs and Y27632 pretreatment of both CHO-IC1-GFP cells and HUVECs did not significantly alter projection formation (Fig. 7, *A* and *B*), despite inducing a marked decrease in the amount of stress fibers present, as assessed by TRITC-phalloidin staining (data not shown).

ICAM-1 projections do not function in firm adhesion

To assess whether the ICAM-1-enriched projections functioned in adhesion strengthening, we subjected K562-LFA-1 cells to static adhesion assays using monolayers of CHO-IC1-GFP cells as the substrate. Basal binding of K562-LFA-1 cells was significantly increased by activation with mAb CBR-LFA1/2 and was reduced by ICAM-1 and LFA-1 blocking mAbs to levels similar to those exhibited by K562 cells (Fig. 8*A*). Despite the significant reduction in projections induced by preincubation of the CHO-IC1-GFP cells with cytochalasin D, BAPTA-AM, and colchicine (Fig. 7), these treatments did not reduce either basal or activated K562-LFA-1 cell adhesion (Fig. 8*A*). To assess adhesion under more specified and physiologic shear conditions, we examined cell resistance to detachment in laminar shear flow. While a regiment of 4 min each of 16, 32, and 64 dyne/cm^2 caused nearly complete detachment of K562-LFA-1 cells pretreated with mAbs to ICAM-1 and LFA-1, pretreatment of CHO-IC1-GFP cells with colchicine did not significantly alter cell detachment compared with control (Fig. 8*B*).

Finally, we examined adhesion of monocytes to MCP-1-treated HUVECs by static adhesion assay. Although Ab blockade of ICAM-1/LFA-1 interactions alone or along with blockade of VCAM-1/VLA-4 significantly reduced adhesion, pretreatment of HUVECs with cytochalasin D, colchicine, or BAPTA-AM failed to reduce adhesion (Fig. 8*C*). Thus, the ICAM-1-enriched projections did not significantly contribute to the strength of leukocyte adhesion.

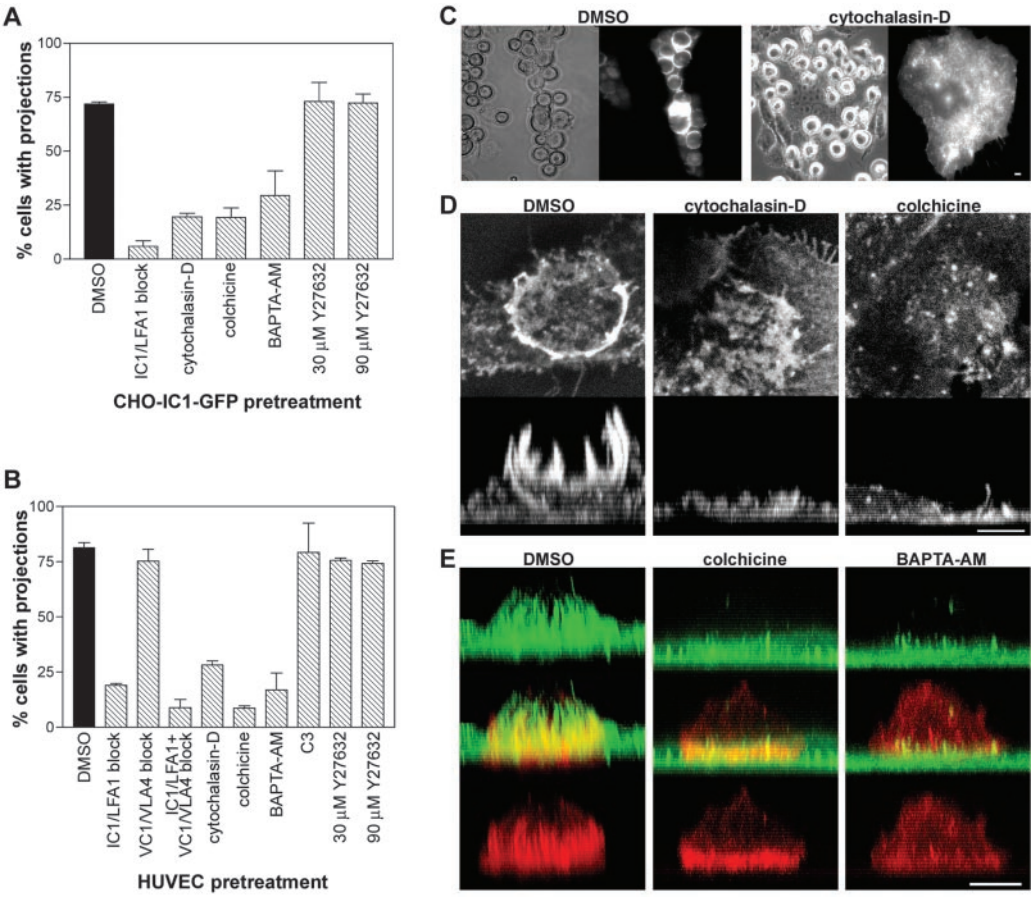

FIGURE 7. Projections require ICAM-1/LFA-1 interactions, intact microfilaments and microtubules, and intracellular calcium in ICAM-1-bearing cells. CHO-IC1-GFP cells (*A* and *C*) or TNF-α-activated CBR-IC1/11–488-Fab-stained HUVECs (*B*, *D*, and *E*) were pretreated with either ICAM-1 (RR1/1) and LFA-1 (TS1/18) blocking mAbs (IC1/LFA1 block), VCAM-1 (BBIG-V1 and 1.G11B1) and VLA-4 (HP2/1) blocking mAbs (VC1/VLA4 block), DMSO, cytochalasin D, colchicine, BAPTA-AM, C3 transferase, or Y27632 as described in *Materials and Methods*. Either Mn^{2+}-activated K562-LFA-1 cells (*A*, *C*, and *D*) or MCP-1-activated monocytes (*B* and *E*) were incubated with the monolayers for 20 min followed by fixation. *A* and *B*, At least 50 adherent cells from randomly selected fields were viewed in all Z-planes and scored for the presence of ICAM-1 projections of at least 1 μm in length. Each bar represents the percentage of total adherent cells scored positive for projections. Values are mean $\pm$ SD from two to three separate experiments. *C*, Representative live cell DIC (*left panels*) and fluorescence (*right panels*) images of DMSO- and cytochalasin D-pretreated CHO-IC1-GFP cells bound to CBR-LFA1/2-activated K562-LFA-1 cells. *D*, Representative top (*upper panels*) and side (*lower panels*) view projections of confocal Z-series of DMSO-, cytochalasin D-, or colchicine-pretreated HUVECs bound to CBR-LFA1/2-activated K562-LFA-1 cells. *E*, Side views of MCP-1-activated monocytes bound to DMSO-, colchicine-, or BAPTA-AM-pretreated HUVECs. ICAM-1 is shown in green and LFA-1 is shown in red. Scale bars, 5 μm.

Discussion

To better understand the roles played by ICAM-1 and LFA-1 in leukocyte/endothelial interactions, we characterized, with high spatial resolution, the distribution dynamics of ICAM-1 and LFA-1. These experiments resulted in five central observations. First, we found that the endothelium rapidly extended ICAM-1-enriched microvilli-like vertical projections in response to LFA-1 engagement, which formed cup-like structures that surrounded adherent leukocytes. Second, projections induced clustering of LFA-1 into linear tracks along the sides of leukocytes. Third, projections were formed by proactive functions provided strictly by the endothelium and not the leukocytes. Fourth, projections were independent of VCAM-1/VLA-4 interactions and shear but required intracellular calcium and intact microfilament and microtubule cytoskeletons in the endothelium. Finally, projections were not found to play a critical role in firm adhesion.

A variety of previously published in vivo electron microscopy studies have also demonstrated formation of "endothelial microvilli" that appear to embrace adherent and transmigrating leukocytes (31–33). Taken together, these studies establish the idea that the leukocyte/endothelial interface takes on a distinct three-dimensional architecture. However, the adhesion receptors, proactive signaling events, and mechanisms important for the formation of this architecture have not been completely characterized. Analysis of endothelial VCAM-1 and, to a lesser extent, ICAM-1 during adhesion of lymphocytes has demonstrated formation of VCAM-1-, ICAM-1-, ezrin- and actin-enriched microvilli-like projections that encircled adherent lymphocytes in a manner likened to a phagocytic cup (25). VCAM-1/VLA-4 interactions were shown to be sufficient for projection formation (25). However, whether ICAM-1/LFA-1 interactions actively participate in projection formations remains unknown. Our studies with K562-LFA-1 cells, which lack VLA-4 expression, and with ICAM-1/LFA-1 and VCAM-1/VLA-4 function blocking Abs demonstrate that ICAM-1/LFA-1 interactions are sufficient to drive formation of ICAM-1-enriched projects independently of VCAM-1/VLA-4 interactions. Furthermore, while the overall morphological results are similar, our findings differ in a number of important respects, including the delineation of the signaling events involved in projection formation and the function of the projections.

To delineate the specific roles played by the leukocyte and the endothelium during ICAM-1 projection formation, we examined

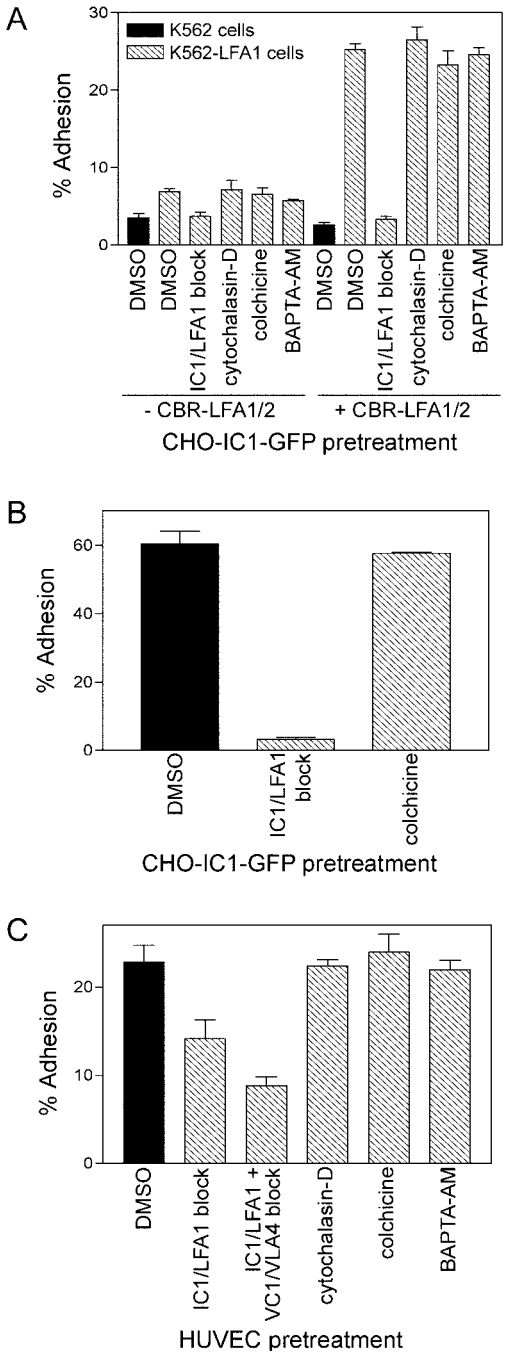

FIGURE 8. Inhibition of ICAM-1 projections by cytochalasin D, colchicine, or BAPTA-AM does not alter firm adhesion. CHO-IC1-GFP cells (*A* and *B*) or TNF-α-activated, MCP-1-pretreated HUVECs (*C*) were pretreated with ICAM-1 (RR1/1) and LFA-1 (TS1/18) blocking mAbs (IC1/LFA1 block), VCAM-1 (BBIG-V1 and 1.G11B1) and VLA-4 (HP2/1) blocking mAbs (VC1/VLA4 block), DMSO, cytochalasin D, colchicine, or BATPTA-AM as described in *Materials and Methods*. *A* and *C*, BCECF-labeled K562 or K562-LFA-1 cells in the absence or presence of CBR-LFA1/2 (*A*) or freshly isolated human monocytes (*C*) were incubated with monolayers in 96-well plates for 20 min at 37°C. Plates were washed and analyzed as described in *Materials in Methods*. Bars represent percentage of input cells that remained adherent after wash steps. Values are mean ± SEM from three separate experiments. *B*, K562-LFA-1 cells were allowed to adhere to CHO-IC1-GFP monolayers plated in a laminar flow chamber for 20 min at 37°C under static conditions. Cells were then detached by a shear regiment of 4 min each of 16, 32, and 64 dyne/cm^2 and adhesion was quantitated as described in *Materials and Methods*. Bars represent the percentage of initially adherent cells that remained adherent at the completion of the shear regiment. Values are mean ± SD for two separate experiments.

the consequences of disruption of cytoskeletal function and calcium signaling selectively in either the leukocytes or the endothelium. Moreover, we compared projection formation induced by K562 cells bearing intact LFA-1 with K562 cells bearing the isolated LFA-1 I domain in the absence of integrin cytoplasmic domains and latex beads coated with anti-ICAM-1 Abs. These experiments demonstrated a complete lack of a role for LFA-1 signaling and for proactive contributions from the leukocytes in the formation of projections, suggesting a critical role for ICAM-1 signaling in the endothelium. By contrast, treatment of the endothelial cells with BAPTA-AM, cytochalasin D, or colchicine resulted in dramatic inhibition of projections. These data suggest important roles for the endothelial cytoskeleton and calcium signaling in projection formation. Thus, it appears that the role of the leukocytes is to cluster ICAM-1, thereby signaling the proactive response of projection formation in the endothelium.

Since Rho signaling has previously been shown to be activated by ICAM-1 clustering (15–17), we examined the effects of Rho and ROCK inhibition on the formation of ICAM-1-enriched projections in CHO-IC1-GFP cells and HUVECs after binding K562-LFA-1 transfectants or monocytes. In our experiments, C3 transferase and Y27632 pretreatments that were comparable to, or at concentrations severalfold higher than, those previously reported to effectively inactivate endothelial Rho and ROCK, respectively (16, 17, 25), caused marked reduction in stress fibers but failed to alter formation of ICAM-1 projections. This contrasts with the previous finding that VCAM-1 projections were destabilized by Y27632 (25). Whether this difference reflects differential requirements for Rho/ROCK signaling in the formation of ICAM-1- and VCAM-1-dependent projections is currently unknown.

To better understand the effect of endothelial ICAM-1 projections on adherent leukocytes, we imaged the distribution of LFA-1 (and Mac-1) in the monocytes and neutrophils using a nonperturbing mAb to the integrin β_2 subunit. These experiments revealed a striking organization of the integrin β_2 subunit along the sides and over the tops of the leukocytes into linear clusters that mirrored the vertical tracks of the ICAM-1 projections. Such vertical LFA-1 clusters were absent when ICAM-1 projections were inhibited, demonstrating their dependence on these endothelial structures. The precise cellular consequences of this LFA-1 patterning is currently unclear. However, it is conceivable that it could function in establishing proper leukocyte polarity during TEM (10, 11). Indeed, the geometry of the integrin substrate can significantly influence the position in which cells initiate filopodia and lamellipodia extension and hence the direction in which they move (34), an effect which may be related to the ability of ligand-bound integrins to specifically localize CDC42 and Rac activity (10).

To address the role of ICAM-1 projections in firm adhesion, we conducted static adhesion assays in 96-well plates and controlled detachment assays in a laminar flow chamber. By design, experimental treatments had no effect on the opportunity of cells to initially interact with and adhere to the ICAM-1-bearing cells, affording an unambiguous assessment of the relative strengths of the adhesions formed. Our data show that three distinct agents that each produced significant inhibition of projections were incapable of producing quantitatively significant alterations in adhesion strength. These data are consistent with a variety of previous studies, which similarly found that endothelial pretreatment with cytochalasin D, BAPTA-AM (16, 18, 20), or colchicine (J. Greenwood and P. Adamson, personal communication) did not effect leukocyte adhesion. Furthermore, if projections served a critical role in adhesion strengthening, one might expect to see an asymmetric development of projections under shear forces, such that

those projections oriented to bear the most load would be exaggerated compared with those that are not. However, when projections were formed under 4 dyne/cm^2, a substantial shear force, no such asymmetry was observed. In addition, the kinetics of projection formation are inconsistent with a role in arrest and are not in good agreement with a role in adhesion strengthening, events that take place on a time scale of fractions or 10s of seconds, respectively (35). Thus, despite the attractive appearance of the projections as adhesion strengthening structures, our results, coupled with a variety of previous studies, demonstrate that the endothelial projections do not play a critical role in adhesion strengthening. The previous suggestion that VCAM-1 projections might contribute to adhesion strengthening was based on a rolling assay, in which rolling, adhesion, and TEM are all highly interdependent (25). Since the observed reduction in adhesion under conditions that destabilized VCAM-1 projections was accompanied by a similar, and in fact slightly greater, reduction in rolling (an effect that was attributed by the authors to events distinct from projection formation), these experiments were inconclusive.

Our observations are consistent with a potential role for the projections in the process of TEM. In contrast to their lack of effect on firm adhesion, all of the treatments, which we found to inhibit endothelial projections (cytochalasin D, colchicine and BAPTA-AM), have previously been found to specifically inhibit TEM (Refs. 16, 18, and 20; J. Greenwood and P. Adamson, personal communication). Moreover, the kinetics of projection formation are in excellent agreement with a role in TEM, which occurs on a time scale of minutes (35). Finally, in the course of these studies we have found that ICAM-1 projections appear to be associated with leukocytes throughout the process of TEM (C.V.C and T.A.S., unpublished observations). Thus, the formation of ICAM-1-enriched cup-like structures by the endothelium appears to be intimately associated with TEM.

Acknowledgments

We thank Dr. Thomas Vorup-Jensen for the many useful discussions and for his careful reading of this manuscript.

References

1. Luscinskas, F. W., G. S. Kansas, H. Ding, P. Pizcueta, B. E. Schleiffenbaum, T. F. Tedder, and M. A. Gimbrone, Jr. 1994. Monocyte rolling, arrest and spreading on IL-4-activated vascular endothelium under flow is mediated via sequential action of L-selectin, β_1-integrins, and β_2-integrins. *J. Cell Biol. 125:1417*.
2. Springer, T. A. 1994. Traffic signals for lymphocyte recirculation and leukocyte emigration: the multi-step paradigm. *Cell 76:301*.
3. Greenwood, J., Y. Wang, and V. L. Calder. 1995. Lymphocyte adhesion and transendothelial migration in the central nervous system: the role of LFA-1, ICAM-1, VLA-4 and VCAM-1. *Immunology 86:408*.
4. Luscinskas, F. W., H. Ding, and A. H. Lichtman. 1995. P-selectin and vascular cell adhesion molecule 1 mediate rolling and arrest, respectively, of CD4$^+$ T lymphocytes on tumor necrosis factor α-activated vascular endothelium under flow. *J. Exp. Med. 181:1179*.
5. Oppenheimer-Marks, N., L. S. Davis, D. T. Bogue, J. Ramberg, and P. E. Lipsky. 1991. Differential utilization of ICAM-1 and VCAM-1 during the adhesion and transendothelial migration of human T lymphocytes. *J. Immunol. 147:2913*.
6. Reiss, Y., G. Hoch, U. Deutsch, and B. Engelhardt. 1998. T cell interaction with ICAM-1-deficient endothelium in vitro: essential role for ICAM-1 and ICAM-2 in transendothelial migration of T cells. *Eur. J. Immunol. 28:3086*.
7. Weber, C. and T. A. Springer. 1998. Interaction of very late antigen-4 with VCAM-1 supports transendothelial chemotaxis of monocytes by facilitating lateral migration. *J. Immunol. 161:6825*.
8. Wong, D., R. Prameya, and K. Dorovini-Zis. 1999. In vitro adhesion and migration of T lymphocytes across monolayers of human brain microvessel endothelial cells: regulation by ICAM-1, VCAM-1, E-selectin and PECAM-1. *J. Neuropathol. Exp. Neurol. 58:138*.
9. Calderwood, D. A., S. J. Shattil, and M. H. Ginsberg. 2000. Integrins and actin filaments: reciprocal regulation of cell adhesion and signaling. *J. Biol. Chem. 275:22607*.
10. Del Pozo, M. A., W. B. Kiosses, N. B. Alderson, N. Meller, K. M. Hahn, and M. A. Schwartz. 2002. Integrins regulate GTP-Rac localized effector interactions through dissociation of Rho-GDI. *Nat. Cell Biol. 4:232*.
11. Worthylake, R. A., and K. Burridge. 2001. Leukocyte transendothelial migration: orchestrating the underlying molecular machinery. *Curr. Opin. Cell Biol. 13:569*.
12. Dustin, M. L., and T. A. Springer. 1988. Lymphocyte function associated antigen-1 (LFA-1) interaction with intercellular adhesion molecule-1 (ICAM-1) is one of at least three mechanisms for lymphocyte adhesion to cultured endothelial cells. *J. Cell Biol. 107:321*.
13. Carpen, O., P. Pallai, D. E. Staunton, and T. A. Springer. 1992. Association of intercellular adhesion molecule-1 (ICAM-1) with actin-containing cytoskeleton and α-actinin. *J. Cell Biol. 118:1223*.
14. Heiska, L., K. Alfthan, M. Gronholm, P. Vilja, A. Vaheri, and O. Carpen. 1998. Association of ezrin with intercellular adhesion molecule-1 and -2 (ICAM-1 and ICAM-2): regulation by phosphatidylinositol 4,5-bisphosphate. *J. Biol. Chem. 273:1893*.
15. Thompson, P. W., A. M. Randi, and A. J. Ridley. 2002. Intercellular adhesion molecule (ICAM)-1, but not ICAM-2, activates RhoA and stimulates c-fos and rhoA transcription in endothelial cells. *J. Immunol. 169:1007*.
16. Adamson, P., S. Etienne, P. O. Couraud, V. Calder, and J. Greenwood. 1999. Lymphocyte migration through brain endothelial cell monolayers involves signaling through endothelial ICAM-1 via a rho-dependent pathway. *J. Immunol. 162:2964*.
17. Etienne, S., P. Adamson, J. Greenwood, A. D. Strosberg, S. Cazaubon, and P. O. Couraud. 1998. ICAM-1 signaling pathways associated with Rho activation in microvascular brain endothelial cells. *J. Immunol. 161:5755*.
18. Etienne-Manneville, S., J. B. Manneville, P. Adamson, B. Wilbourn, J. Greenwood, and P. O. Couraud. 2000. ICAM-1-coupled cytoskeletal rearrangements and transendothelial lymphocyte migration involve intracellular calcium signaling in brain endothelial cell lines. *J. Immunol. 165:3375*.
19. Durieu-Trautmann, O., N. Chaverot, S. Cazaubon, A. D. Strosberg, and P. O. Couraud. 1994. Intercellular adhesion molecule 1 activation induces tyrosine phosphorylation of the cytoskeleton-associated protein cortactin in brain microvessel endothelial cells. *J. Biol. Chem. 269:12536*.
20. Huang, A. J., J. E. Manning, T. M. Bandak, M. C. Ratau, K. R. Hanser, and S. C. Silverstein. 1993. Endothelial cell cytosolic free calcium regulates neutrophil migration across monolayers of endothelial cells. *J. Cell Biol. 120:1371*.
21. Pfau, S., D. Leitenberg, H. Rinder, B. R. Smith, R. Pardi, and J. R. Bender. 1995. Lymphocyte adhesion-dependent calcium signaling in human endothelial cells. *J. Cell Biol. 128:969*.
22. Su, W. H., H. I. Chen, J. P. Huang, and C. J. Jen. 2000. Endothelial $[Ca^{2+}]_i$ signaling during transmigration of polymorphonuclear leukocytes. *Blood 96:3816*.
23. Sandig, M., E. Negrou, and K. A. Rogers. 1997. Changes in the distribution of LFA-1, catenins, and F-actin during transendothelial migration of monocytes in culture. *J. Cell Sci. 110:2807*.
24. Wojciak-Stothard, B., L. Williams, and A. J. Ridley. 1999. Monocyte adhesion and spreading on human endothelial cells is dependent on Rho-regulated receptor clustering. *J. Cell Biol. 145:1293*.
25. Barreiro, O., M. Yanez-Mo, J. M. Serrador, M. C. Montoya, M. Vicente-Manzanares, R. Tejedor, H. Furthmayr, and F. Sanchez-Madrid. 2002. Dynamic interaction of VCAM-1 and ICAM-1 with moesin and ezrin in a novel endothelial docking structure for adherent leukocytes. *J. Cell Biol. 157:1233*.
26. Klickstein, L. B., and T. A. Springer. 1995. CD54 (ICAM-1) cluster report. In *Leucocyte Typing V: White Cell Differentiation Antigens.* S. F. Schlossman, L. Boumsell, W. Gilks, J. Harlan, T. Kishimoto, T. Morimoto, J. Ritz, S. Shaw, R. Silverstein, T. Springer, Tet al., eds. Oxford Univ. Press, New York, p. 1548.
27. Lu, C., M. Shimaoka, Q. Zang, J. Takagi, and T. A. Springer. 2001. Locking in alternate conformations of the integrin $\alpha_L\beta_2$ I domain with disulfide bonds reveals functional relationships among integrin domains. *Proc. Natl. Acad. Sci. USA 98:2393*.
28. Lu, C., M. Shimaoka, M. Ferzly, C. Oxvig, J. Takagi, and T. A. Springer. 2001. An isolated, surface-expressed I domain of the integrin $\alpha_L\beta_2$ is sufficient for strong adhesive function when locked in the open conformation with a disulfide. *Proc. Natl. Acad. Sci. USA 98:2387*.
29. Ulmer, A. J., and H. D. Flad. 1979. Discontinuous density gradient separation of human mononuclear leucocytes using Percoll as gradient medium. *J. Immunol. Methods 30:1*.
30. Cinamon, G., V. Shinder, and R. Alon. 2001. Shear forces promote lymphocyte migration across vascular endothelium bearing apical chemokines. *Nat. Immunol. 2:515*.
31. Faustmann, P. M., and R. Dermietzel. 1985. Extravasation of polymorphonuclear leukocytes from the cerebral microvasculature: inflammatory response induced by α-bungarotoxin. *Cell Tissue Res. 242:399*.
32. Fujita, S., R. K. Puri, Z. X. Yu, W. D. Travis, and V. J. Ferrans. 1991. An ultrastructural study of in vivo interactions between lymphocytes and endothelial cells in the pathogenesis of the vascular leak syndrome induced by interleukin-2. *Cancer 68:2169*.
33. Raine, C. S., B. Cannella, A. M. Duijvestijn, and A. H. Cross. 1990. Homing to central nervous system vasculature by antigen-specific lymphocytes. II. Lymphocyte/endothelial cell adhesion during the initial stages of autoimmune demyelination. *Lab. Invest. 63:476*.
34. Parker, K. K., A. L. Brock, C. Brangwynne, R. J. Mannix, N. Wang, E. Ostuni, N. A. Geisse, J. C. Adams, G. M. Whitesides, and D. E. Ingber. 2002. Directional control of lamellipodia extension by constraining cell shape and orienting cell tractional forces. *FASEB J. 16:1195*.
35. Luu, N. T., G. E. Rainger, and G. B. Nash. 1999. Kinetics of the different steps during neutrophil migration through cultured endothelial monolayers treated with tumour necrosis factor-α. *J. Vasc. Res. 36:477*.